Patterns, Impacts, and Future Projections of Summer Variability in the Arctic from CMIP5 Models

LEI CAI

International Arctic Research Center, University of Alaska Fairbanks, Fairbanks, Alaska, and NORCE Norwegian Research Centre, and Bjerknes Centre for Climate Research, Bergen, Norway

VLADIMIR A. ALEXEEV AND JOHN E. WALSH

International Arctic Research Center, University of Alaska Fairbanks, Fairbanks, Alaska

UMA S. BHATT

Department of Atmospheric Sciences, University of Alaska Fairbanks, Fairbanks, Alaska

(Manuscript received 1 March 2018, in final form 2 October 2018)

ABSTRACT

Thirty models in phase 5 of the Coupled Model Intercomparison Project (CMIP5) are evaluated for their performances in reproducing two summertime atmospheric circulation patterns in the Arctic: the Arctic Oscillation (AO) and Arctic dipole (AD). The reference AO and AD are extracted from the ERA-Interim dataset (1979–2016). Model evaluation is conducted during the historical period (1901–2005). Models are ranked by a combined metrics approach based on two pattern correlation coefficients (PCCs) and two explained variances for the AO and AD, respectively. In the projected period (2006–2100), most models produce a positive trend for the AO index and a negative trend for the AD index in summer. The models ranked higher based on the combined metrics ranking show greater consistency and smaller values in the magnitudes of trends of AO and AD than the lower-ranked ones. The projected trends in the AO and AD contribute to a slight increase, if not a decrease, of the air temperature and an acceleration of precipitation increase in the twenty-first century over Arctic Alaska, which is the reverse of over the Barents and Kara Seas. Changes in the AO and AD are relatively minor contributing factors to the projected temperature and precipitation changes in the Arctic, among which the changes in the AD play a bigger role than those in the AO. The summer AO and AD have a stronger impact on the spatial asymmetry of the precipitation field than on the air temperature field.

1. Introduction

Two leading modes—the Arctic Oscillation (AO) and the Arctic dipole (AD)—contribute the most to the large-scale atmospheric circulation over the Arctic in summer [June–August (JJA)]. By definition, both modes of variability are derived from applying empirical orthogonal function (EOF) analysis to the sea level pressure (SLP) anomaly field. The first EOF mode represents the AO that dominates the atmospheric circulation over the Arctic (Thompson and Wallace 1998; Wu et al. 2006), while the second EOF mode represents the AD (Wu et al. 2006; Watanabe et al. 2006). Some other names and variants for the AD include the Barents oscillation (Skeie 2000; Tremblay 2001), the transpolar drift (Gudkovich 1961), and the Arctic rapid change pattern (ARP; X. Zhang et al. 2008).

The AO can be interpreted as the modulation in the strength of the polar vortex manifested at the surface and drives atmospheric mass exchange between the Arctic and midlatitudes by strengthening or weakening the jet stream, resulting in larger anomalies of precipitation and temperature over the midlatitudes than the Arctic (Thompson and Wallace 1998; Deser 2000). Compared to the annular-shaped pattern of the winter AO, the summer AO has a similar spatial pattern that is

Supplemental information related to this paper is available at the Journals Online website: https://doi.org/10.1175/JCLI-D-18-0119.s1.

Corresponding author: Lei Cai, lcai4@alaska.edu

DOI: 10.1175/JCLI-D-18-0119.1

smaller in size and weaker in magnitude (Wang and Ikeda 2000). The negative AO in the summer and the corresponding anticyclonic wind anomaly contribute to a reduction in sea ice extent in the following September (Ogi et al. 2016). As more observations of sea ice are available, it has become apparent that the AO alone is unable to fully explain the wind-driven sea ice advection (Rigor et al. 2002; Wu et al. 2006).

While the AD is neither as strong (in terms of the variance explained) nor as stable (in terms of reproducibility) as the AO, its associated circulation anomaly has played a significant role in sea ice decline (Watanabe et al. 2006; Wang et al. 2009). Several studies have found that the positive AD's transpolar anomalous wind can drive sea ice export from the Chukchi–eastern Siberia regions; for example, the sea ice plummet event in the summer of 2007 that opened a large water area over the Beaufort and Chukchi Seas (J. Zhang et al. 2008; Wang et al. 2009; Overland et al. 2012; Zhang 2015). A model-based study by J. Zhang et al. (2008), concluded that only 30% of the sea ice retreat is attributed to the sea ice advection, while 70% results from the amplified melting of sea ice, which is due to the preconditioning of thin sea ice and the sea surface heating. Steele et al. (2010) further found that the solar radiation is the main contributor (80%) to such amplified sea ice melting in the Beaufort and Chukchi Seas. As evidence, anomalously low cloudiness was indeed observed by both ground and satellite observations over the Pacific sector of the Arctic Ocean in the summer of 2007 (Kay et al. 2008; Kay and Gettelman 2009). Although detailed mechanisms are still unclear, such a decrease in cloud cover and amplified surface heating may have a physical relationship with the positive AD that represents an anomalous mode of atmospheric circulation pattern.

While the positive AD's anomalous meridional wind in summer results in sea ice advection from the Pacific sector to the Atlantic sector of the Arctic Ocean (Wu et al. 2006, 2012), a positive AD is also likely to lead to a drier and warmer summer over northern coastal Alaska. The positive AD of the summer of 2007 contributed to the outbreak of tundra fires in 2007 over the North Slope of Alaska (Alexeev et al. 2015). X. Zhang et al. (2008) have suggested that the AD is an important driver of the rapid climate changes across the whole pan-Arctic in the first decade of the twenty-first century, as the shift in this atmospheric circulation pattern helps accelerate the gradual changes by the global warming.

Global climate models (GCMs) have become a powerful tool to study the large-scale atmospheric circulation patterns and their climatic impacts, especially with the fact that those patterns and the associated climatic variability may change under the warming climate background. Based on the EC-EARTH model, van der Linden et al. (2017) suggested a colder Arctic associated with a positive phase of the AO in a $2 \times CO_2$ scenario, which is contrary to the current observational results. Empowered by GFDL CM2.1, Zhang (2015) concluded that the AD is one of the keys to predicting the Arctic sea ice extent in summer. The present study aims to investigate whether GCMs can reasonably reproduce AO and AD patterns and the corresponding climatic impacts, thereby providing guidance for selecting models for the projection of atmospheric circulation changes over the Arctic and their corresponding impacts. This study focuses on a suite of models from phase 5 of the Coupled Model Intercomparison Project (CMIP5; Taylor et al. 2012), assembling the latest generation of global climate/Earth system models that served the Fifth Assessment Report (AR5) of the Intergovernmental Panel on Climate Change (IPCC).

As the population of GCMs increases, the need to evaluate GCMs for their performance in reproducing climate variability also becomes greater. As the previous generation of CMIP5, the CMIP3 models have been evaluated in terms of major climatic variabilities and have been found to be more successful in retrieving the spatial patterns than the temporal indices (Xin et al. 2008; Stoner et al. 2009). Regarding the CMIP5 model evaluation, the Community Earth System Model (CESM) working group has developed a climate variability diagnostics package (CVDP; http://www.cesm.ucar.edu/working_groups/CVC/cvdp). The CVDP serves as a platform for evaluations of CMIP5 models for their performances in reproducing the modes of climate variability, as well as the corresponding temperature and precipitation anomalies (Phillips et al. 2014). Some of the most important modes of variabilities, for example, the AO in winter, are quantitatively compared with each other by involving the parameters of the pattern correlation coefficient and the root-mean-square difference. Given the importance of the summer atmospheric circulation patterns for the Arctic climate change, the quantitative evaluation of the summer AO and AD in CMIP5 models in this study provides a timely complement to other CVDP results.

Model-based studies have demonstrated that the climate variability in the Arctic is subject to change in response to external forcing, for example, anthropogenic greenhouse gases (Yukimoto and Kodera 2005; Miller et al. 2006; Choi et al. 2010). A question, therefore, raised along with the model evaluation is how the climate variability reproduced by the relatively successful models, as well as its climatic impacts, changes through time by the end of twenty-first century. In this paper, we develop a combined metrics ranking approach

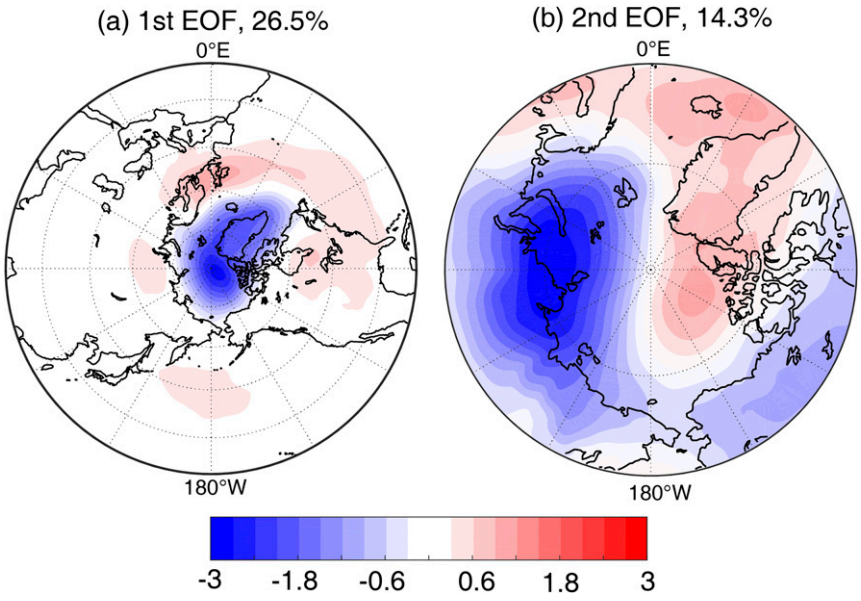

FIG. 1. The spatial patterns of JJA (a) AO and (b) AD in ERA-Interim in the period of 1979–2016. The AO is presented as the first EOF mode of SLP poleward to 20°N, while the AD is presented as the second EOF mode of SLP poleward to 60°N.

to rank 30 CMIP5 models on how well they perform in depicting the AO and AD in summer in the historical period (1901–2005). We also examine the evolution of the summer AO and AD in the projected period (2006–2100), seeking an ensemble of the climatic impacts of the summer AO and AD in the Arctic through the end of the twenty-first century among the group of more successful models. This study aims to answer the following questions:

- How well do CMIP5 models represent the patterns of AO and AD in summer, as well as their impacts on the temperature and precipitation fields?
- How do model-produced patterns and climatic impacts of the summertime AO and AD change in the twenty-first century? Do these changes depend on the models' performance during the historical period?
- How do the summertime AO and AD jointly contribute to the Arctic climate change in the twenty-first century? Which climatic mode plays a more important role?

2. Methodology

a. Reanalysis data and CMIP5 model products selection

We evaluate CMIP5 models with the ERA-Interim dataset (Dee et al. 2011) as the reference climate. Although the ERA-Interim is 30 years shorter in temporal coverage compared to the NCEP–NCAR reanalysis that has been used in some previous evaluations (Deser 2000; Kistler et al. 2001; Stoner et al. 2009; Overland et al. 2012), ERA-Interim's higher spatial resolution (T255; roughly 80 km) and the advanced four-dimensional variation data assimilation (4D-Var) have built its foundation to retrieve more accurate precipitation and temperature fields than the NCEP–NCAR reanalysis does in the Arctic (Lindsay et al. 2014), which is essential for this study in addition to reproducing reasonable patterns of the AO and AD. ERA-Interim's summertime (JJA) AO and AD patterns and indices are reasonable and similar to those in NCEP–NCAR reanalysis data (Fig. 1; the AD pattern in the NCEP–NCAR reanalysis is shown in the online supplemental material). The ERA-Interim-produced summer AO and AD, respectively, explain 26.5% and 14.3% of the total variance in SLP anomaly over their respective domain (20°–90°N for the AO and 60°–90°N for the AD).

Thirty CMIP5 models are evaluated over the historical period (1901–2005, Table 1). They are the subset of all CMIP5 models for which the output datasets meet the two following criteria: 1) the monthly averaged variables in both historical and representative concentration pathway 8.5 (RCP8.5) experiments are available to download via the Earth System Grid Federation (ESGF) from the node of Lawrence Livermore National Laboratory (http://esgf-node.llnl.gov/projects/esgf-llnl), and 2) the model is included in the CVDP CMIP5 historical experiment evaluation. CVDP does not quantitatively compare the summer AO performance in CMIP5 models, while the climatic impacts of the summer AO

TABLE 1. The list of chosen CMIP5 models in this study.

No.	Model	Atmospheric grid resolution (°)	Institution
1	ACCESS1.0	1.875 × 1.25	Commonwealth Scientific and Industrial Research Organization, and Bureau of Meteorology, Australia
2	ACCESS1.3		
3	CCSM4	1.25 × 0.9	National Center for Atmospheric Research
4	CESM1(CAM5)		National Science Foundation Department of Energy National Center for Atmospheric Research
5	CanESM2	2.81 × 2.79	Canadian Centre for Climate Modelling and Analysis
6	CMCC-CM	0.75 × 0.75	Centro Euro-Mediterraneo sui Cambiamenti Climatici
7	CMCC-CMS	3.75 × 3.71	
8	CNRM-CM5	1.41 × 1.40	Centre National de Recherches Météorologiques/Centre Européen de Recherche et de Formation Avancée en Calcul Scientifique
9	CSIRO-Mk3.6.0	1.875 × 1.86	Commonwealth Scientific and Industrial Research Organization in collaboration with the Queensland Climate Change Centre of Excellence
10	GFDL-ESM2G	2.0 × 2.0	Geophysical Fluid Dynamics Laboratory
11	GFDL-ESM2M	2.5 × 2.0	
12	GISS-E2-H	2.5 × 2.0	NASA Goddard Institute for Space Studies
13	GISS-E2-H-CC		
14	GISS-E2-R		
15	GISS-E2-R-CC		
16	HadGEM2-AO	1.875 × 1.25	Met Office Hadley Centre
17	HadGEM2-CC		
18	HadGEM2-ES		
19	INMCM4	2.0 × 1.5	Institute for Numerical Mathematics
20	IPSL-CM5A-LR	3.75 × 1.9	Institut Pierre-Simon Laplace
21	IPSL-CM5A-MR	2.5 × 1.26	
22	IPSL-CM5B-LR	3.75 × 1.9	
23	MIROC5	1.41 × 1.40	Atmosphere and Ocean Research Institute, National Institute for Environmental Studies, and Japan Agency for Marine-Earth Science and Technology
24	MIROC-ESM	2.81 × 2.79	Japan Agency for Marine-Earth Science and Technology, Atmosphere and Ocean Research Institute, and National Institute for Environmental Studies
25	MIROC-ESM-CHEM		
26	MPI-ESM-LR	1.875 × 1.86	Max Planck Institute for Meteorology
27	MRI-CGCM3	1.125 × 1.125	Meteorological Research Institute
28	MRI-ESM1		
29	NorESM1-M	2.5 × 1.9	Norwegian Climate Centre
30	NorESM1-ME		

differ significantly from those of the winter [December–February (DJF)] AO (Ogi et al. 2016). We utilize the model output from only the first ensemble member of each model for a consistent comparison, as for some models only the first ensemble member output is available to download. Such selection is also consistent with that in CVDP, which enables the comparison between their evaluation results and ours. The first ensemble member of RCP8.5 projections of the same 30 models are also downloaded for the evolutions of the summertime AO and AD in the twenty-first century. When involved in quantitative comparisons or constructing multimodel composites, data from reanalysis datasets and models are regridded to the same 1.875° × 1.25° grid (192 × 145 grid points). Such grid resolution is close to the median resolution of the chosen CMIP5 models, ensuring a fair comparison.

b. *Calculation of AO/AD in CMIP5 models*

In this study, the methodology of defining the AO and AD is consistent with the previous studies (Thompson and Wallace 1998; Watanabe et al. 2006). The AO is defined as the first EOF mode of the area-weighted (multiplied by square root of the cosine of latitude) SLP anomalies over the region poleward of 20°N (20°–90°N, 180°E–180°W). The AD usually appears as the second EOF of SLP that is calculated in the same way as AO but over a smaller region (poleward of 60°N). The corresponding (first and second) principal components (PCs) represent the time series (indices) of the AO and the AD.

The AO, as the dominant mode of climatic variability in the Arctic, consistently appears in the first mode of EOF. However, the dipole-shaped pattern representing the AD may not appear until the third or fourth EOF mode for some models, in which case the explained variance is typically low. Therefore, we keep employing the first EOF mode as the AO pattern, while searching for the dipole-shaped pattern representing the AD from the second to fifth EOF modes. Each model produces its own AO and AD (as we will see later in the text) with geographically differing patterns, which makes a comparison of the corresponding PCs with reanalysis results also across models, difficult, if not impossible. Furthermore, spatial EOF patterns and the corresponding PC time series are somewhat dependent on the period in which the EOF analysis is addressed. To avoid this problem, this study obtains the model-produced AO and AD indices by regressing the summer SLP anomalies in CMIP5 models onto the spatial patterns of AO and AD produced by ERA-Interim data (Fig. 1). Thus, the model-produced AO and AD indices correspond consistently to the same spatial patterns of AO and AD produced by ERA-Interim, which has been proved to represent the reasonable dynamics of the AO and AD in summer. Defining the model-produced AO and AD indices in this way eliminates the dependence on the spatial and temporal coverage of the EOF analysis input data. It builds consistency when comparing the responses of other climatic variables (e.g., precipitation and temperature) between models corresponding to the indices. The Climate Prediction Center of the National Weather Service (http://www.cpc.ncep.noaa.gov/products/precip/CWlink/daily_ao_index/ao.shtml) has employed a similar methodology in routinely updating the daily and monthly AO index. Correspondingly, the impacts of AO and AD on precipitation and temperature fields are calculated by regressing the AO and AD indices that are obtained in the way mentioned above onto the anomalies of precipitation and temperature.

c. Model evaluation

We rank the models by introducing the pattern correlation coefficient (PCC) and the explained variance obtained from the EOF analysis. The PCC quantifies the similarity of a pair of gridded spatial patterns, having been widely applied to evaluate the numerical weather forecast skill (Murphy and Epstein 1989; Ebert and McBride 2000; Krishnamurti et al. 2003). Langland and Maue (2012) employed this approach to compare the skills of forecasting the AO in winter between multiple numerical weather prediction systems. The PCCs in this study are calculated by the following formula:

$$\mathrm{PCC} = \frac{\sum_{i=1}^{N} F_i R_i}{\left[\sum_{i=1}^{N} (\mathrm{F})_i^2 \sum_{i=1}^{N} (R_i)^2\right]^{1/2}}, \tag{1}$$

in which F_i and R_i are, respectively, the EOF grid point values from the CMIP5 model and the ERA-Interim dataset after the regridding. The summations are performed over N grid points. It is worth noting that the calculation of PCC for the AO integrates a larger number of grid points than that of the AD (poleward of 20°N vs poleward of 60°N).

A combined metrics ranking method calculates the combined deviation of the vector of multiple m parameters from the reference. The combined metrics score is calculated by the following formula:

$$S = \sqrt{\sum_{i=1}^{m} (\Delta P_i)^2}, \tag{2}$$

in which ΔP_i is the difference between the ith model parameter (PCCs and explained variances of both the AO and AD, in this case) and the corresponding reference parameter. Before calculating the combined metric score, a feature-scaling method normalizes each of the vector components by rescaling the range of the sample to 1 using the formula as follows in order to equalize the weight of each individual parameter:

$$x' = \frac{x}{\max(x) - \min(x)}, \tag{3}$$

where $\max(x)$ and $\min(x)$ are, respectively, the largest and the smallest values in the sample. The parameters for calculating the combined metrics score are the PCCs and the explained variances of both the AO and AD. The model with the lowest score is ranked the highest. The PCCs for the reference AO and AD are 1 by definition. Note that such combined metrics ranking actually incorporates unequal weights to the AO and AD, as the AD is calculated in a smaller domain (60°–90°N) than the AO is (20°–90°N). These unequal weights, however, do not significantly affect the ranking. Detailed discussion is addressed in the discussion section and supplemental material.

The root-mean-square error (RMSE) in this study calculated from the biases of all grid points quantifies the difference in spatial patterns between the CMIP5 models and ERA-Interim. However, RMSE is not involved as one parameter in the combined metrics ranking, as by definition it is significantly inversely correlated to the PCC. Involving both the PCC and

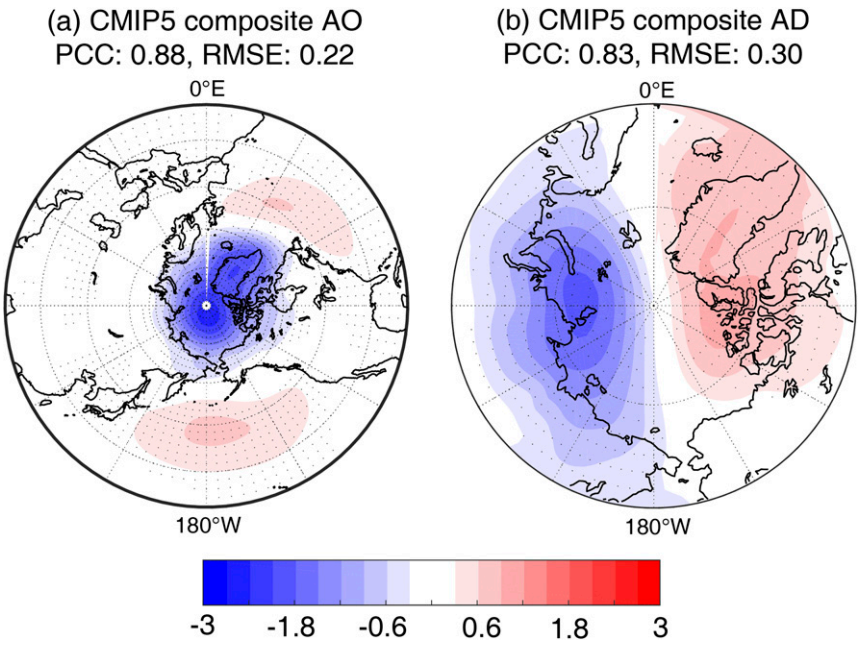

FIG. 2. The CMIP5 model composite patterns of JJA (a) AO and (b) AD. Regions with black dots indicate the anomaly values in composite members exceed the 95% significance level using the Student's *t* test.

RMSE would give overly high weight to the spatial pattern compared to the explained variance. Alternatively, the RMSE serves as the tiebreaker that a higher rank is given to the model with a lower RMSE among the ones with identical combined metric scores. PCCs and RMSEs are also calculated for the regressed temperature and precipitation in each model (listed in the supplemental material), but only to show a quantification of the similarity of spatial patterns of impacts, rather than to rank the models. Stoner et al. (2009) have found it much harder for GCMs to reasonably reproduce the temporal spectra of indices than to reproduce their spatial patterns. We, therefore, excluded the temporal variabilities of the summertime AO and AD from our rankings and focused our scope specifically on the spatial metrics.

3. Results

a. *Evaluation of summer AO and AD in CMIP5 historical products*

The selected CMIP5 models are evaluated regarding their ability to reproduce the summer AO and AD. The PCCs and explained variances quantify the similarity between the model-produced and the reference AO and AD, to which a score is given by a combined metrics ranking. The lower the combined metrics score, the better the model performs on reproducing the summer climatic variabilities over the Arctic. The 30-model composite of the AO and AD patterns in summer are compared with those in ERA-Interim in the main body of text, while the summer AD patterns of each individual model are depicted in the supplemental material.

1) SPATIAL PATTERN COMPARISONS

Although without quantitative comparisons, the summer AO patterns visualized by CVDP (http://webext.cgd.ucar.edu/Multi-Case/CVDP_ex/CMIP5-Historical/nam.jja.png) exhibit that most models are able to produce an annular-shaped pattern resembling the AO in summer with a negative anomaly over the central Arctic and two positive anomalies, respectively, over the North Pacific and the North Atlantic. Such spatial distribution is similar to that of AO in winter, but with a smaller amplitude (Ogi et al. 2016). The CMIP5 model composite for the summer AO presents an annular-shaped pattern, as in our EOF analysis, also with negative anomaly centers over the central Arctic and two positive anomalies over the North Pacific and North Atlantic, respectively (Fig. 2a). This anomaly distribution matches that of the ERA-Interim well, with a PCC of 0.88 and an RMSE of 0.22.

The model composite pattern of the summer AD successfully exhibits the dipole shape, with the PCC of 0.83 and RMSE of 0.30 (Fig. 2b). Twenty-seven models are able to reproduce the dipole-shaped pattern spatially

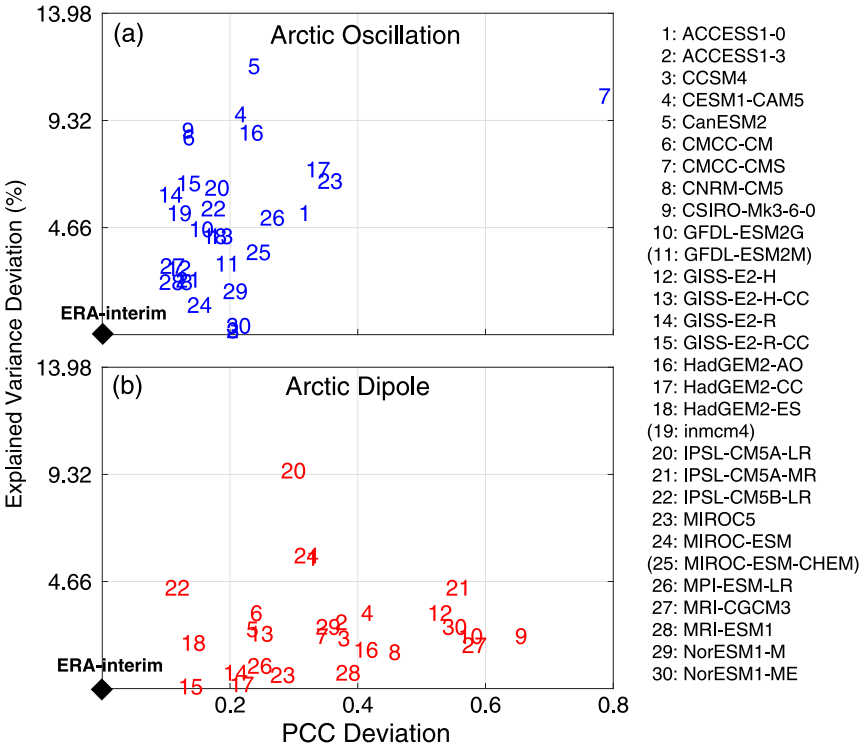

FIG. 3. The deviations of PCC and explained variance of model-produced summer (a) AO and (b) AD patterns from the reference (ERA-Interim). The models corresponding to the numbers in the figures are listed on the right. Models with names in parentheses fail to reproduce the dipole-shaped pattern of the AD.

in a certain (second to fifth) EOF mode, while three models [GFDL-ESM2M; Institute of Numerical Methods of the Russian Academy of Sciences, Climate Model, version 4 (INMCM4); and MIROC-ESM-CHEM] fail to present it in the first five EOF modes (spatial patterns of the AD for all 27 models are shown in the supplemental material). These three models, therefore, tie at the twenty-eighth place without conducting the combined metrics ranking for a score (Table 2). Among the other 27 models, 14 of them resolve the AD pattern in the second EOF mode, and 9 out of 10 models that resolve the AD pattern in the third EOF mode have the explained variances higher or very close (9.9%) to 10%, which is very close to the 14 models above. Two models (ACCESS1.0 and IPSL-CM5A-LR) do not resolve the AD pattern until the fourth EOF mode, with the explained variances as low as 8.5% and 4.8%, respectively.

2) MODEL RANKING

The PCCs and explained variances of the model-produced AO and AD are applied to conduct the combined metrics ranking, before which the relative performance of CMIP5 models in the summer AO and AD are examined and compared separately (Fig. 3). Most models are able to produce highly correlated (PCC $>$ 0.8) spatial patterns of the AO, while they differ from each other mostly on the explained variance (Fig. 3a). In contrast, the model-produced AD has larger differences in the PCCs than in the explained variances, despite the fact that three models fail to reproduce the summer AD and are not included in Fig. 3b. While most models are clustered together, there is one outlier that emerges in the evaluation of each of the two modes: CMCC-CMS for the AO and IPSL-CM5A-LR for the AD. They diverge from the other models for different reasons. The summer AO pattern in CMCC-CMS has three negative anomalies: over the Aleutian Islands, Greenland, and the Barents Sea instead of one over the central Arctic (the relative figure is shown on the CVDP website). The AD in IPSL-CM5A-LR that is resolved in the fourth EOF mode has a much lower explained variance (4.8%) than other models (Table 2; spatial pattern is shown in the supplemental material). HadGEM2-ES is ranked as the best model with a combined metrics score of 0.402, followed by the three models in the GISS model family (GISS-E2-R-CC, GISS-E2-R, and GISS-E2-H-CC). The two outliers, respectively, in the AO and AD evaluation, CMCC-CMS and IPSL-CM5A-LR, rank as number 27 and number 25. The top 25% (top seven) models have the combined metrics scores below 0.6.

TABLE 2. The list of the explained variances, PCCs, and RMSEs of the 30 models on AO and AD, which is sorted by the overall rank (descending) considering both the AO and AD in the leftmost column.

		AO			AD				
Rank	CMIP5 model	Explained variance (%)	PCC	RMSE	EOF mode resolves AD	Explained variance (%)	PCC	RMSE	Combined metrics score
1	HadGEM2-ES	22.2	0.84	0.27	Second	16.3	0.88	0.26	0.402
2	GISS-E2-R-CC	19.9	0.88	0.21	Second	14.2	0.88	0.27	0.435
3	GISS-E2-R	20.4	0.91	0.18	Second	15.0	0.81	0.33	0.464
4	GISS-E2-H-CC	22.2	0.83	0.26	Third	11.9	0.77	0.35	0.518
5	IPSL-CM5B-LR	21.0	0.85	0.27	Third	9.9	0.90	0.24	0.542
6	MPI-ESM-LR	21.4	0.75	0.36	Second	13.3	0.77	0.36	0.558
7	MRI-ESM1	28.8	0.91	0.17	Second	13.6	0.64	0.45	0.594
8	NorESM1-M	28.4	0.81	0.26	Second	11.6	0.67	0.43	0.624
9	HadGEM2-CC	19.3	0.68	0.39	Second	14.5	0.80	0.33	0.649
10	CCSM4	26.7	0.81	0.27	Second	16.5	0.63	0.45	0.650
11	ACCESS1.3	26.7	0.81	0.30	Third	11.4	0.64	0.44	0.665
12	CMCC-CM	17.9	0.87	0.24	Third	11.0	0.77	0.37	0.677
13	MIROC-ESM	25.2	0.87	0.24	Third	8.5	0.70	0.42	0.701
14	MIROC5	19.8	0.66	0.44	Second	13.7	0.74	0.40	0.703
15	CNRM-CM5	24.2	0.88	0.24	Second	12.7	0.55	0.49	0.735
16	CanESM2	14.8	0.77	0.32	Third	11.7	0.78	0.36	0.821
17	HadGEM2-AO	17.7	0.79	0.33	Second	16.0	0.61	0.47	0.838
18	ACCESS1.0	21.2	0.69	0.46	Fourth	8.6	0.68	0.43	0.848
19	GISS-E2-H	23.6	0.90	0.21	Third	11.0	0.49	0.50	0.861
20	NorESM1-ME	26.1	0.81	0.27	Third	11.6	0.47	0.54	0.891
21	CESM1(CAM5)	16.9	0.79	0.28	Third	11.0	0.60	0.48	0.908
22	MRI-CGCM3	29.5	0.91	0.17	Second	12.4	0.44	0.54	0.909
23	IPSL-CM5A-MR	24.1	0.89	0.21	Third	9.9	0.46	0.51	0.934
24	GFDL-ESM2G	21.9	0.86	0.26	Second	16.6	0.44	0.53	0.936
25	IPSL-CM5A-LR	32.9	0.84	0.29	Fourth	4.8	0.72	0.39	1.002
26	CSIRO-Mk3.6.0	17.6	0.88	0.22	Second	16.6	0.36	0.58	1.143
27	CMCC-CMS	16.1	0.22	0.83	Third	12.0	0.67	0.45	1.279
28	GFDL-ESM2M	23.4	0.82	0.28	—	—	—	—	—
28	INMCM4	21.2	0.90	0.19	—	—	—	—	—
28	MIROC-ESM-CHEM	30.1	0.78	0.34	—	—	—	—	—

Applying EOF analysis on the summer SLP anomaly field over the region 20°–90°N, a dipole-shaped pattern representing the AD remains in the central Arctic in the third or fourth EOF mode (depending on the reanalysis or GCM and period chosen). Two extra SLP anomaly centers are over the south of the Bering and Fram Straits, respectively. The Atlantic multidecadal oscillation (AMO) and PDO are the two major climatic modes of variability with decadal to multidecadal scales of oscillation over these two target regions. To further explore the role of low-frequency modes of variability, a linear correlation analysis was performed between the ranks solely on the summer AD (ranked by the distance from ERA-Interim to models; Fig. 3b) and the PCCs/RMSEs of both monthly AMO and monthly PDO that is calculated by CVDP (Fig. 4). While the RMSEs show little correlation to the rank of the AD, the PCCs of both the AMO and PDO do visually show some negative linear correlation to the rank of the AD, meaning that models that perform better in reproducing the summer AD also perform better in producing the spatial patterns of the monthly AMO and PDO. Statistically, the level of significance for the correlation between the rank of the AD and the PCC of AMO is close to 90%.

b. *Summer temperature and precipitation regressed on AO and AD*

To explore models' performances regarding the impacts of AO and AD, the model-produced summertime temperature and precipitation anomalies are regressed onto the AO and AD indices, which are calculated by regressing the SLP anomalies onto the AO and AD patterns in ERA-Interim. The similarity between the temperature and precipitation pattern of a certain model and that of ERA-Interim is quantified by the PCCs and RMSEs. The CMIP5 model composite obtained by averaging the regression fields of all included CMIP5 models is shown in Figs. 5 and 6, while spatial patterns for each individual model, as well as the PCCs and RMSEs, are in the supplemental material. Most CMIP5 models are able to reproduce the reasonable spatial distributions of temperature and precipitation

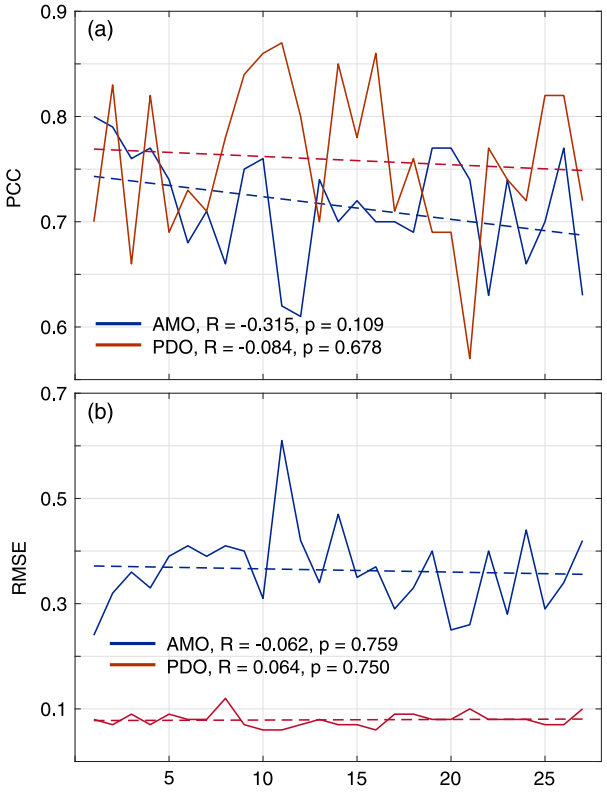

FIG. 4. The (a) PCC and (b) RMSE of model-produced AMO (blue lines) and PDO (red lines) as a function of the model rank based only on summer AD.

impacts resulting from the AO and AD compared to those in the ERA-Interim, although the patterns somewhat differ from each other in the small scale. For CSIRO-Mk3.6.0, we find a flaw in the monthly averaged surface air temperature data in that it remains at 0 K in all the grid points globally from June 1997 to July 1998. Therefore, CSIRO-Mk3.6.0 was also excluded from the temperature regression composites of AO and AD in this study in addition to the three models that fail to reproduce the AD pattern.

For the temperature anomalies regressed on the AO, the CMIP5 model composite agrees with the ERA-Interim that the positive anomalies are mostly over northern Canada and northern Europe, with magnitudes of 0.2°–0.6°C per standard deviation (°C STD^{-1}; Figs. 5a,b). The negative anomalies in the model composite are moderate (<0.4°C STD^{-1}) over northern Alaska, the Kara Sea, and the western coast of Greenland. The ERA-Interim has similar magnitudes of negative anomalies in the above regions, while there are other regions with wider-spread negative anomalies with greater magnitudes (0.3°–0.8°C STD^{-1}), including eastern Siberia, Hudson Bay, southern United States, and the Mediterranean. There are no apparent temperature anomalies over the central Arctic in most cases shown in the composite, except for the ERA-Interim and some models that have small (<0.4°C STD^{-1}) negative anomalies over the Arctic Ocean (the composite pattern is shown in Fig. 5b, while the patterns for individual models are shown in Fig. S3 in supplemental material).

The CMIP5 model composite has a dipole-shaped pattern of temperature anomalies regressed on the AD. The 120°E–60°W meridian, in general, divides the zones of positive and the negative temperature anomalies (Fig. 5d). Positive temperature anomalies are presented over northern Siberia, northern Alaska, and northern Canada, while negative anomalies are located over the coastal regions of the Barents and Kara Seas. The CMIP5 models generally have similar temperature anomaly patterns to ERA-Interim along the pan-Arctic coastal region. For the central Arctic, the CMIP5 model composite shows generally small (<0.4°C STD^{-1}) and insignificant positive temperature anomalies over the eastern Siberia Sea, the Chukchi Sea, and the Beaufort Sea, over which the ERA-Interim shows anomalies close to zero (Fig. 5c).

For monthly precipitation anomalies regressed on the AO, the two patterns of the ERA-Interim and CMIP5 model composite match, while the magnitudes are typically twice as large as those in the model composite (Figs. 6a,b). One exception is over the Arctic Ocean where the CMIP5 model composite and ERA-Interim both show positive anomalies of precipitation in similar magnitude (around 4–6 mm STD^{-1}). They also agree geographically on having a strip-shaped region with negative anomalies crossing through the North Atlantic, Scandinavia, and all the way to central Siberia. ERA-Interim has anomalies of nearly twice the magnitude in this region compared to CMIP5 model composite (up to 8 mm STD^{-1} vs up to 4 mm STD^{-1}). Positive precipitation anomalies are apparent in both CMIP5 model composite and ERA-Interim over eastern Asia, northern India, the oceanic region to the west of Hawaii, and the Gulf of Mexico. Precipitation regressed on the AD shows a dipole-shaped distribution for the CMIP5 model composite, with a neutral line located roughly on the 0°E–180°W meridian (Figs. 6c,d). Positive precipitation anomalies occur along the coast of the Barents and Kara Seas, while negative anomalies occur over northern Alaska, northern Canada, and Greenland. ERA-Interim gives generally a similar distribution, but with more topographical features because of its higher spatial resolution (e.g., opposite precipitation anomalies over the northern and the southern foothills of the Brooks Range in Arctic Alaska). Such detailed topographical features in the ERA-Interim lower the PCCs for some models that

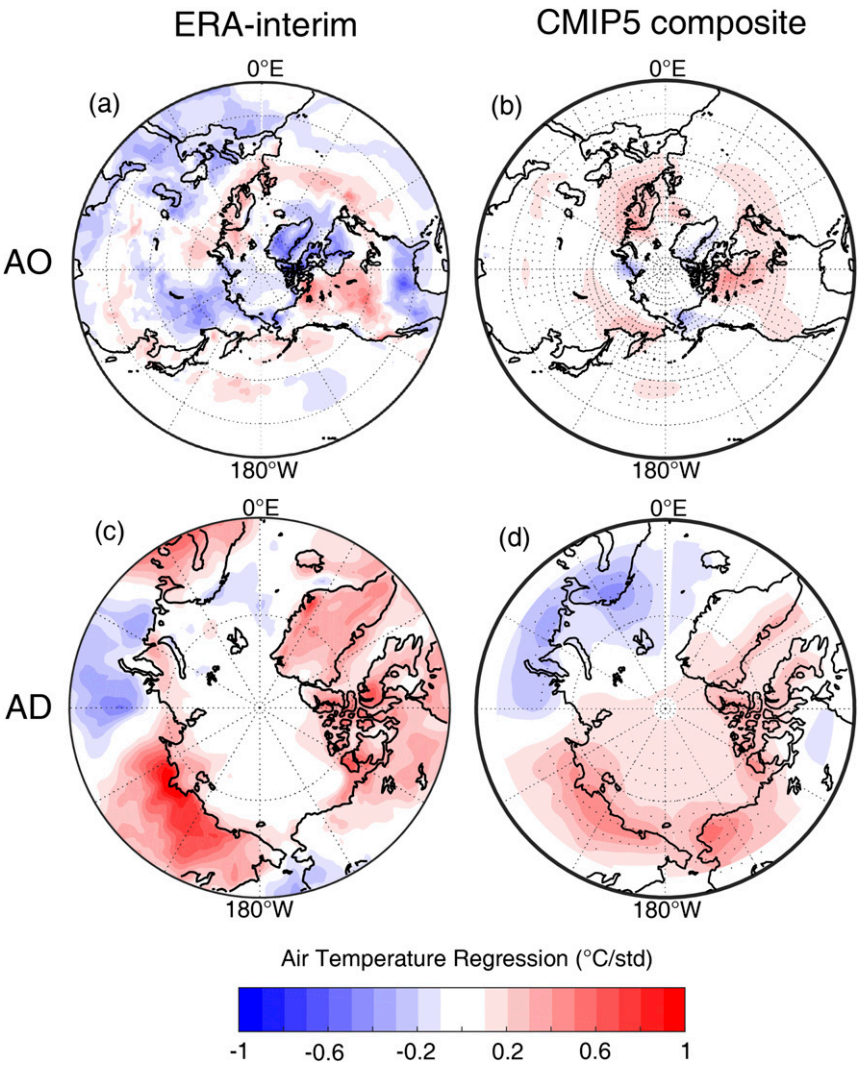

FIG. 5. The JJA temperature and precipitation anomalies regressed on (a),(b) AO and (c),(d) AD indices in (a),(c) ERA-Interim and (b),(d) CMIP5 model composite. Regions with black dots indicate the anomaly values in composite members exceed the 95% significance level using the Student's *t* test.

successfully capture the large-scale anomaly patterns but fail to reproduce small-scale details.

The AO-regressed temperature and precipitation anomalies in CMIP5 models exhibit a stronger signal over the midlatitudes and sub-Arctic than over the central Arctic, being consistent with the physical mechanism of AO, which is the modulation of the strength and wavelength of the jet stream (Thompson and Wallace 1998). The slightly negative SLP anomaly in the central Arctic corresponds to the slight decrease in temperature and increase in precipitation over the Arctic Ocean. Such correspondences may result from more clouds forming in response to the low pressure system that helps to decrease the temperature and bring more precipitation. The greatest model-to-reanalysis disagreement occurs in middle latitudes, for example, over the southern United States and southern Europe.

The regressed temperature and precipitation on the summer AO and AD in both the ERA-Interim and model composite are able to represent the impacts of the AO and AD in summer and are consistent with the results of previous studies. The positive phase of summer AO is associated with warmer northwestern Canada and western Europe and colder eastern Siberia, Alaska, and Baffin Bay (L'Heureux et al. 2010). Associated with the positive AO in summer, precipitation is inhibited over northeastern Canada (Hu and Feng 2010) and central Siberia (Balzter et al. 2005). In the positive phase of the AD, the anomalous meridional wind corresponding to the SLP anomaly brings warm air to the central Arctic

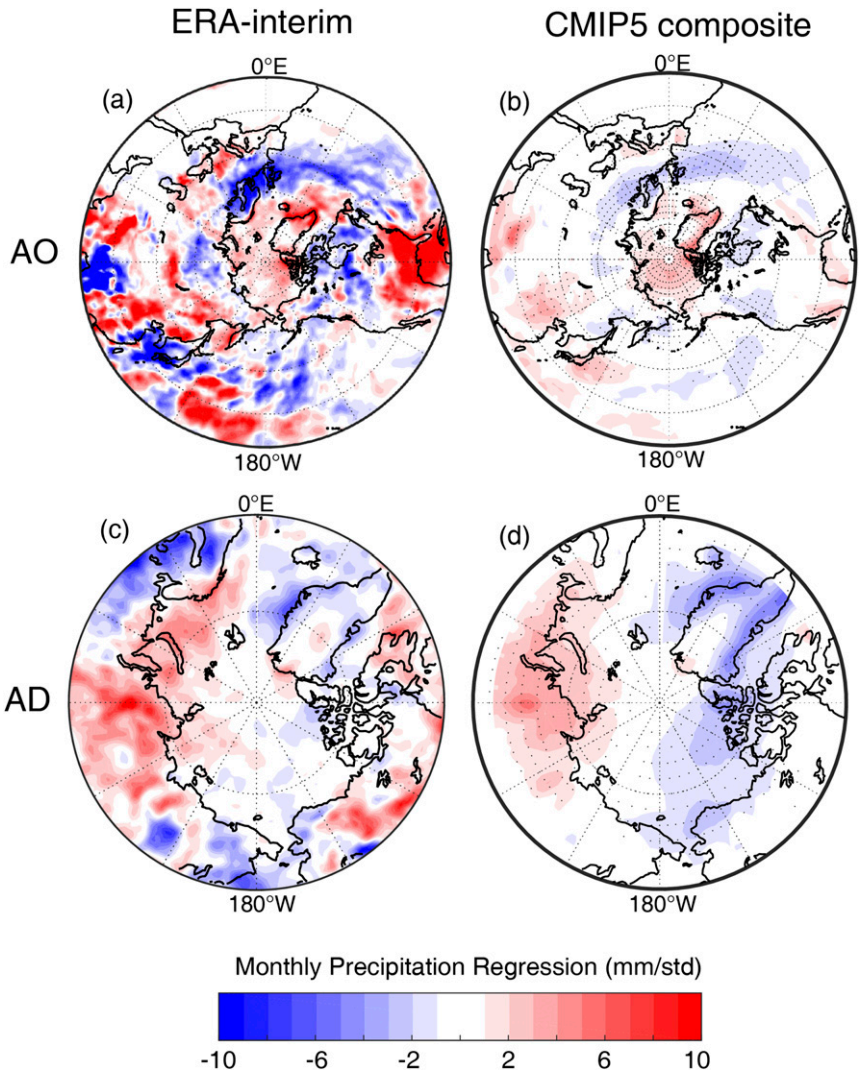

FIG. 6. As in Fig. 5, but for monthly precipitation regressions.

and cold air to the North Atlantic (Watanabe et al. 2006). The AD in its positive phase represents the ensemble of the atmospheric states in which more high pressure systems are found over the Beaufort Sea and northern Canada, and more low pressure systems travel over northern Eurasia (Overland and Wang 2010). Such SLP anomalies can make precipitation inhibited on the North American side, while enhanced on the Eurasian side of the pan-Arctic.

c. *AO and AD in the twenty-first century and their impacts on Arctic climate change*

In concatenated time series of model output for the historical and projected periods, the indices of the AO and AD in the 30 CMIP5 models exhibit oscillations on the multidecadal time scale (Figs. 7a,b). The AO and AD indices in the projected period are calculated by regressing the SLP anomalies in the RCP8.5 experiment onto the AO and AD spatial patterns in ERA-Interim, the same way as calculating the AO and AD indices in the historical period. In the projected period (2006–2100), the most distinct turnaround of the medians of the summer AO and AD indices occurs around the 2030s. Before the 2030s, the median of AO index generally has a decreasing trend, while that of AD index has an increasing trend. After the 2030s, both medians of trends turn to the other way around (increasing trend for the AO, while decreasing trend for the AD). Seeing from the whole projected period (2006–2100), there is only one model with an overall decreasing AO trend and one with increasing AD trend (Fig. 7c). Comparing the projected trends of AO and AD between models as the function of the rank based on the historical evaluation, the higher-ranked models are in more agreement with each other on

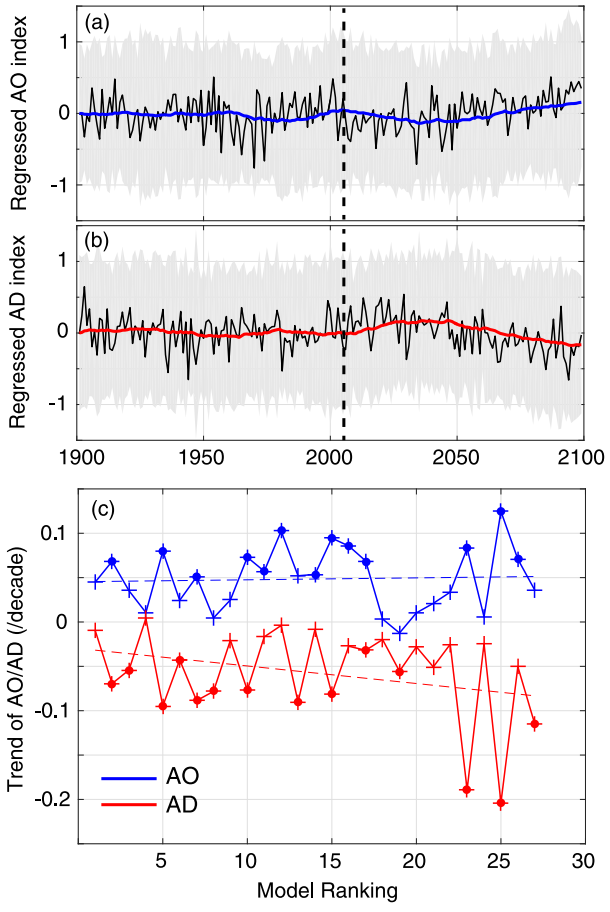

FIG. 7. The medians of (a) AO and (b) AD index from 27 models connecting the historical and projected (RCP8.5) period from 1901 to 2100. The gray-shaded area delimits one standard deviation of the AO or AD index, and the blue or /red lines are the 20-yr moving average of the median time series. (c) The trend of RCP8.5 AO (blue) and AD (red) as the function of the model ranking calculated for the period of 2006–2100. Round markers refer to the significance of the trend via the Mann–Kendall test at the 95% confidence level.

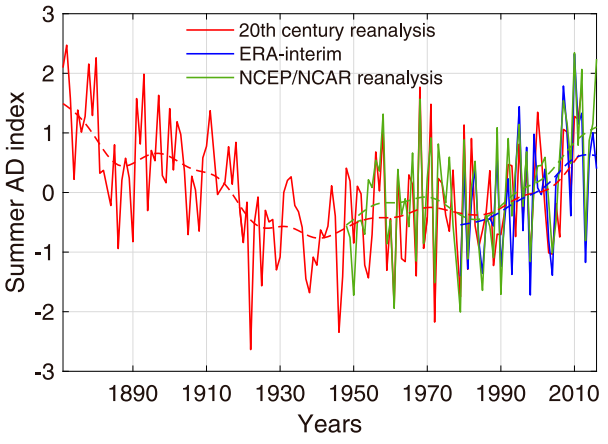

FIG. 8. The JJA AD index derived from the second PC in ERA-Interim (blue), NCEP–NCAR reanalysis (green), and 20CR (red) across their respective temporal coverages, which are 1870–2012 for 20CR, 1948–2016 for NCEP–NCAR reanalysis, and 1979–2016 for ERA-Interim.

the phases and magnitudes of trends than the lower-ranked models are. The increasing AO trend is about 0.05 decade^{-1} on average, while the averaged decreasing AD trend is about -0.06 decade^{-1}. The higher-ranked models typically have smaller magnitudes of trends (absolute value) than the lower-ranked models for both the summer AO and AD indices (Fig. 7c).

The two-century-long composite of the model-produced summer AD index exhibits multidecadal-scale oscillations (Fig. 7b), among which the crest and trough of the longest oscillation occur in the 1940s and 2030s, respectively, with superimposed shorter-term (20–40 years) oscillations. Regarding the AD in reanalysis datasets, both ERA-Interim and NCEP–NCAR have too-short temporal coverages to retrieve the full oscillation with the longest cycle, showing monotonically increasing trends. The Twentieth Century Reanalysis, version 2 (20CR), data (Compo et al. 2011) are able to retrieve a low-frequency oscillation, with a minimum of the summer AD around the late 1930s following a long decreasing trend back to 1871 (Fig. 8). Note that little to no observational data on SLP over the Arctic are assimilated into 20CR prior to the 1930s, bringing more uncertainty to the 20CR-produced AD index before the 1930s (Compo et al. 2011).

In view of the dependence of the trends on model ranks, we pick the models in the top 25th percentile, which are ranked first to seventh, as the representative models for the further exploration of how the projected change of summer AO and AD may contribute to the regional climate change in the Arctic through the end of the twenty-first century. Among the top seven models, around half of models have significant trends of AO and AD calculated over the entire projection period (2006–2100), despite that, the trends of these seven models are typically smaller in magnitude than those of the lower-ranked models. Such agreement and the significance of trends in top models indirectly verify that their projected changes of the AO and AD are more trustworthy than the other models with lower ranks.

The composite trends of summer temperature and precipitation from the top seven models are higher across the pan-Arctic coastal region than over the central Arctic (Figs. 9a,b). Summer temperature over the pan-Arctic coast increases at a rate of more than 0.5°C decade^{-1}, while it increases at about 0.2°C decade^{-1} over the Arctic Ocean. The highest rate of temperature increase (0.8°C decade^{-1}) is over the Barents and

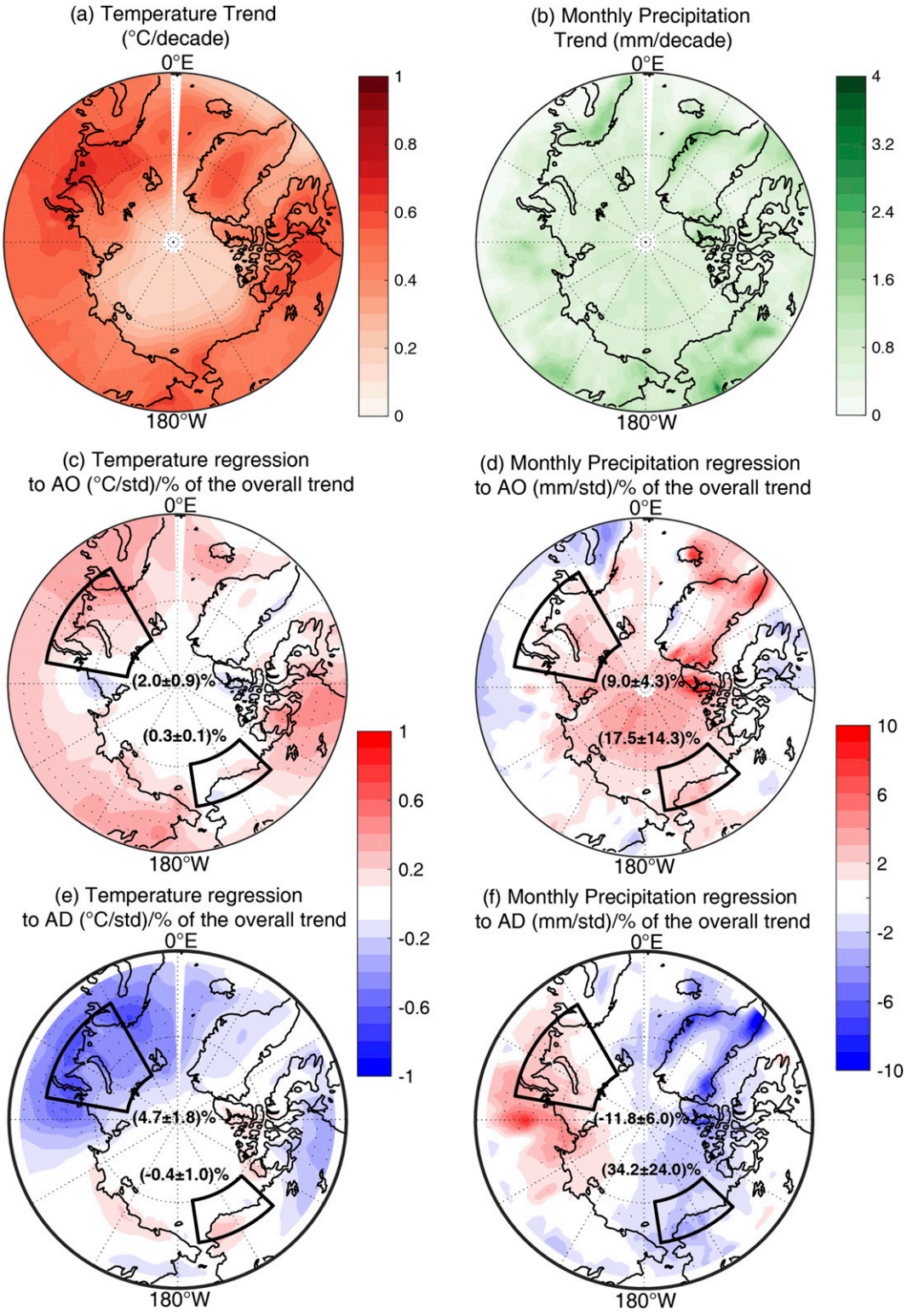

FIG. 9. The composite trend of (a) temperature and (b) precipitation in the top seven models. (c)–(f) The composite of these seven models in regressed (c),(e) temperature and (d),(f) precipitation on AO and AD. Black lines denote the subregions used to examine the contributions independently from AO and AD on temperature and precipitation trends in the top seven models. The uncertainty after the ± sign is one standard deviation of the contribution. Regions with black dots indicate the anomaly values in composite members exceed the 95% significance level using the Student's *t* test.

Kara Seas. The monthly precipitation increases at a rate of 1 mm decade^{-1} or more over most regions. Over 2 mm decade^{-1} of monthly precipitation increase is found over regions like interior Alaska, coastal Greenland, Scandinavia, and north-central Siberia.

Such spatial unevenness of temperature and precipitation changes is attributed partially to the trends of AO and AD in the twenty-first century. Figures 9c–f display the composites of summer temperature and precipitation anomalies regressed on the twenty-first-century AO and AD indices from the top seven models. The spatial patterns of the regressed temperature and precipitation in RCP8.5 projections generally resemble those from the historical period (Figs. 5, 6). We marked two subregions of interest (the black-line delimited regions in Figs. 9c–f), Arctic Alaska (66°–75°N, 130°–170°W) and the Barents Sea (63°–80°N, 30°–75°E), in which the greatest summer precipitation and temperature increases over the pan-Arctic are found, respectively (Figs. 9a,b). The AO- and AD-regressed anomalies of temperature and precipitation over these two subregions are also large (Figs. 5, 6). The impact of the long-term changes of the AO and AD indices to temperature and precipitation is quantified as the product of the trend of AO and AD and the regressed temperature and precipitation anomaly. A comparison between such impacts and the overall changes of temperature and precipitation (Figs. 9a,b) gives the relative contributions by the AO and AD within the regions of interest (percentages in Figs. 9c–f), which is calculated by the following formula:

$$P = \frac{T_i R_v}{T_v} \times 100\%, \tag{4}$$

where T_i is the trend of the AO or AD index (STD decade^{-1}), R_v is the temperature (°C STD^{-1}) or precipitation (mm STD^{-1}) regressed onto the AO or AD, and T_v is the overall trend of temperature (°C STD^{-1}) or precipitation (mm STD^{-1}). Consequently, P stands for the percentage of the temperature or precipitation trend resulting solely from AO or AD.

The fields of these percentages show that the AO's contribution to the increases of the temperature and precipitation in both regions is generally small except for the precipitation over Arctic Alaska (17.5% ± 14.3%). Less than 3% to nearly 0% (2.0% ± 0.9% and 0.3% ± 0.1%) of summer temperature increase results from the AO for both regions (Figs. 9c–f). It is worth noting that the AO trend actually affects the temperature change oppositely over the terrestrial and oceanic regions in the subdomain of Arctic Alaska. Although unclear on the map (Fig. 7c), the calculated relative contribution values of the AO trend are negative (temperature decrease) over land (the Alaskan North Slope), while positive (temperature increase) over the ocean (the Beaufort Sea). The AO contributes to the precipitation increase at a higher rate than to the temperature increase. The trend of AO contributes slightly to the precipitation increase over the Barents Sea with a high uncertainty (9.0% ± 4.3%), while the AO's contribution, as well as the uncertainty, is higher (17.5% ± 14.3%) for the precipitation increase over Arctic Alaska.

The trend of AD influences the temperature and precipitation oppositely in the two regions of interest. The AD accounts for −0.4% ± 1.0% of the summer temperature change over Arctic Alaska, implying, among the different members of this seven-model subset, there are largely offsetting contributions of the AD to the temperature change over this area. Over the Barents Sea, the AD trend facilitates the temperature increase in summer contributing 4.7% ± 1.8% of the total warming. The summer AD explains 11.8% ± 6.0% of the overall decrease of precipitation over the Barents Sea, while it is responsible for 34.2% ± 24.0% of precipitation increase over Arctic Alaska. It means that, for Arctic Alaska, the trend of summer AO and AD together is likely to contribute more than half of the projected summer precipitation change in the twenty-first century, while for other regions (and for temperature in all regions), the trends of AO and AD are still minor contributors.

The association of the positive AD and the anomalous low sea ice extent and total cloud cover, which has been found and analyzed by several observational studies focused on the sea ice plummet in 2007 (Kay et al. 2008; Kay and Gettelman 2009; J. Zhang et al. 2008), were also examined in the reanalysis datasets and top seven models. As the result, the positive phase of the AD in both reanalysis datasets (ERA-Interim and NCEP–NCAR reanalysis, 1979–2016) is associated to the reduction of total cloud fraction over the east Siberian Sea, and that of sea ice concentration over the Pacific sector of the Arctic Ocean (Figs. 10a–d). Similar regressions are generally present in the top seven CMIP5 model composites in the RCP8.5 projection from 2006 to 2050, even though the reduction of cloud fraction is not as apparent as in the reanalysis datasets (Figs. 10e,f). The sea ice concentration distribution regressed on the summer AD is consistent with the associated transpolar wind (Watanabe et al. 2006; Wang et al. 2009; Overland and Wang 2010) and the transpolar-wind-driven sea ice drift (Vihma et al. 2012), where the most convergence of sea ice is found along the Fram Strait. Such sea ice loss in the Beaufort and Chukchi Seas can lead to abrupt increases of temperature and humidity in the following early winter over Arctic Alaska proved by regional

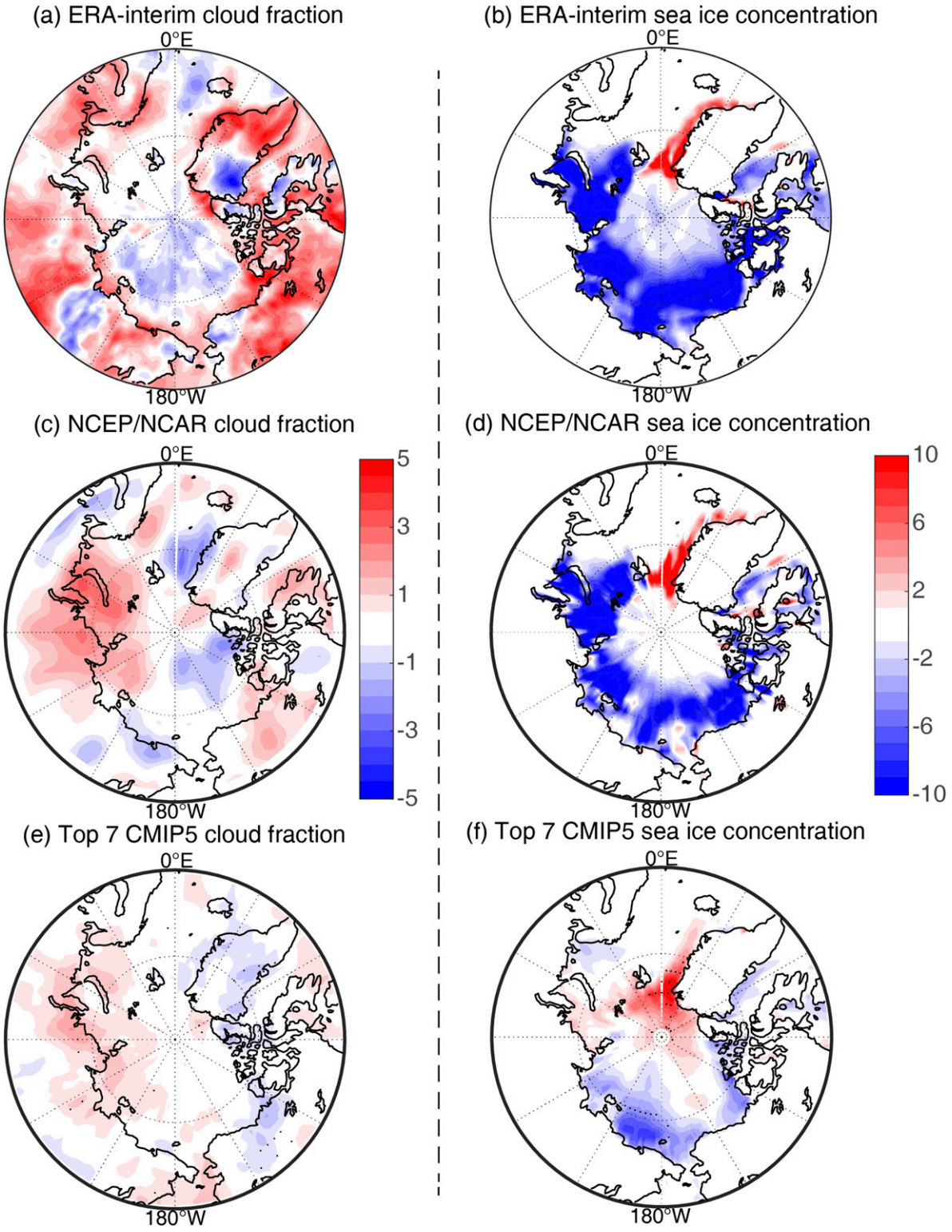

FIG. 10. The spatial distributions of (a),(c),(e) total cloud fraction (%) and (b),(d),(f) sea ice concentration (%) regressed onto AD from (a),(b) ERA-Interim (1979–2016); (c),(d) NCEP–NCAR reanalysis data (1979–2016); and (e),(f) the top seven CMIP5 model composite (2006–50). Regions with black dots indicate the anomaly values in composite members exceed the 95% significance level using the Student's *t* test.

climate simulations (Porter et al. 2012; Cai et al. 2018). We do not include the second half of the twenty-first century, as the RCP8.5 scenario usually projects a close-to-zero sea ice concentration in summer after 2050 (Collins et al. 2013).

4. Discussion

Climate variations are often characterized in terms of the repeated patterns and cycles, which represent the internal variability in the coupled GCMs (Phillips et al. 2014). These patterns and cycles have implications for the future changes of climate conditions, which is why the performance in reproducing climatic variability has become an important factor when evaluating GCMs (Stoner et al. 2009). For the AO and AD, that represent the mass and heat exchange within the Arctic and between the Arctic and the midlatitudes, they play an important role in the linkage of the Arctic and global climate changes (Deser 2000; Wu et al. 2008). Both the AO and AD represent major modes of variability in the Arctic. However, the AD has not been analyzed at depth in CMIP5 models. Our quantitative evaluation of the AO and AD in the summer thus complements the analysis done by CVDP. As CVDP quantifies the PCCs/RMSEs of the wintertime AO, we compare it with our evaluation results to see whether the CMIP5 models have consistent performance in reproducing the AO in summer and in winter. According to CVDP, 29 out of 30 models we selected are able to reproduce the winter AO patterns with PCC $>$ 0.8, and 18 of the models have PCC $>$ 0.9. The CMCC-CMS fails to reproduce a reasonable AO pattern in summer (PCC = 0.225), while it is one of the best models in terms of the AO pattern in winter (PCC = 0.97). This comparison illustrates the fact that a model's performance for the same climatic mode of variability can vary by season, and it is typically more difficult to reproduce climatic variabilities that are less prominent (e.g., the summer AO and AD). A threshold of PCC = 0.6 is interpreted as the lower limit of a practical forecast when PCC was introduced as a metric of forecast skill (Hollingsworth et al. 1980). Out of 30 models, in this case, 20 meet the above standard in reproducing the summer AD pattern that, as noted above, has been overlooked in previous CMIP5 model evaluations.

We include the explained variances in the model evaluation, while CVDP focuses only on the PCCs/RMSEs. CVDP probably needs to have a universal methodology that is also applicable to other variabilities that are not derived from EOF analysis, such as ENSO and the AMO, while the relatively narrow scope of this study allows us to emphasize the importance of the explained variance that mathematically describes the relative contribution of each individual EOF mode to the anomaly field. We regard the explained variance to be as important of a metric as the PCC, especially in the case of the AD, for which the explained variance can vary substantially from model to model. We assign the same weight to the PCC and the explained variance in the combined metric ranking, even though such equal weights may overly exaggerate the importance of explained variance.

In this study, the combined metrics ranking is conducted in the period of 1901–2005 in order to match the chosen period in CVDP. It is worth noting that the mathematics of EOF analysis determines that the EOF patterns and the correspondingly explained variances are dependent on the spatial domain and temporal period of the input data field. The sensitivities of the combined metrics ranking approach are tested in the supplemental material in terms of the chosen domain, period, and reanalysis dataset as the reference. First, the summer AO is calculated within the same domain as the AD (60°–90°N), guaranteeing the same weights of the AO and AD in calculating the combined metrics score, to test the sensitivity of the chosen domain. Then, the whole period (1901–2005) is split into two (1901–50 and 1951–2005), within each one of which the combined metrics ranking is applied. It tests the sensitivity of the combined metrics ranking to the internal variability. In this study, we were more interested in intermodel performance and the stability in the ranking of the top-performing models. One other potential approach to thoroughly testing the sensitivity of EOF modes could be the employment of one of the large ensemble projects, for example, the CESM Large Ensemble (CESM-LENS; Kay et al. 2015). As the result, most of the top models (top seven models in Table 2) consistently fill the top positions in the new rankings conducted using the split periods or a smaller domain for the AO, though their relative positions often switch. The less successful models (e.g., the bottom 25%), on the other hand, remain at similar positions in the new rankings. Similar consistency also exists in examining the ranking based on another reference reanalysis dataset [the ECMWF twentieth century reanalysis (ERA-20C); Poli et al. 2016]. Although it still has room for further improvement, the combined metrics ranking has been proven to be a robust approach and competent to serve for the purpose of this study, which is to screen out a group of better-performing models in reproducing the summer AO and AD (more details are in the supplemental material).

The summer AD index is found to have an oscillation at the multidecadal scale, both in reanalysis datasets and CMIP5 models. Furthermore, it is possible for the AD to

have physical links to the AMO and PDO, implied by the performance of CMIP5 models. These preliminary results are potentially informative to further studies on the dynamics and physical mechanisms of the AD. As we have verified that a number of models are able to reproduce a reasonable AD pattern, one approach may be employing these GCMs for sensitivity experiments with prescribed sea surface temperature (SST) over the North Atlantic and/or North Pacific that imitates the behavior(s) of the AMO and/or PDO.

Under the climate background in the twenty-first century, both the AO and AD in summer change as projected by the CMIP5 models. The CMIP5 models examined by us project positive trends for the AO, which is generally consistent with the studies using a subset of CMIP3 models in the historical period to explore the response of the AO index to the anthropogenic greenhouse gases (Yukimoto and Kodera 2005; Miller et al. 2006). In this study, the model-produced summer AD decreases in the projected period, which is expected to play a bigger role than the increasing trend of the AO in influencing the temperature and precipitation changes in the Arctic. The projected trends of both the summertime AO and AD indices generate stronger impacts on precipitation than on temperature. In terms of the overall climate change over the pan-Arctic coastal regions in summer, the temperature increases faster over the Barents Sea than over Arctic Alaska, while the precipitation increases more rapidly over Arctic Alaska than over the Barents Sea (Figs. 9a,b). Even so, the AO and AD together play a minor role in causing Arctic climate changes in the twenty-first century, as examined in some of the more successful CMIP5 models. Other potentially important contributing factors may include the radiative forcing and Arctic sea ice decline. For example, the large increasing temperature trend over the Barents and Kara Seas in the top seven models (Fig. 9a) may as well be the consequence of the larger open water area in winter and spring driven by the positive AO (Steele et al. 2008).

5. Conclusions

This study evaluates the performances of 30 CMIP5 models in reproducing the AO and AD in summer. Of the 30 models, 29 reproduce reasonable AO patterns in summer, although their pattern correlation coefficients to the reference dataset (ERA-Interim) are not as high as for their AO patterns in winter. Meanwhile, 27 models are able to retrieve a dipole-shaped pattern of the AD in summer, among which 20 models identify the AD in the second EOF mode as in the reference (ERA-Interim). The combined metrics ranking approach involving both the PCC and explained variance of the AO and AD ranks HadGEM2-ES, three GISS models (GISS-E2-R-CC, GISS-E2-R, and GISS-E2-H-CC), IPSL-CM5B-LR, MPI-ESM-LR, and MRI-ESM1 as the group of more successful models, which are in the top 25th percentile. The model-produced temperature and precipitation anomalies brought by the summer AO and AD resembles those in ERA-Interim dataset in the large scale. The positive summer AO brings greater magnitudes of temperature and precipitation anomalies to the mid- to high latitudes than to the central Arctic, while the temperature and precipitation regressed on summer AD present the dipole-shaped patterns. The two-century-long time series of the model-produced AO and AD indices concatenating the historical period and the RCP8.5 projection period show multidecadal-scale oscillations. CMIP5 models project a monotonically increasing AO and a decreasing AD after the 2030s until the end of the twenty-first century. The more successful models show more consistency in the positive trend of the AO and negative trend of the AD, implying that the CMIP5 models that are more successful in capturing the dynamics of summer AO and AD tend to agree more with each other in projecting the changes of AO and AD in the twenty-first century. Such agreement is helpful in selecting model(s) for further studies aimed at future changes in atmospheric circulation pattern and their impacts over the Arctic.

In the twenty-first century, the top seven CMIP5 models project increases for both the summertime air temperature and precipitation over the pan-Arctic (poleward of 60°N) under the RCP8.5 scenario. For the region of Arctic Alaska, the air temperature increases more slowly, while the precipitation increases faster than over the Beringia regions nearby in summer. On the other hand, the Barents Sea has the most air temperature increase and the least precipitation increase around the pan-Arctic in summer. The future change of the AO and AD play a minor role in driving the regional climate change over the pan-Arctic coastal region by the end of twenty-first century, as their relative contributions to the temperature and precipitation changes are less than 10% in most cases. Compared between the AO and AD, the AD drives larger spatial variability of temperature and precipitation in summer than the AO does within the pan-Arctic regions, playing a more important role in influencing the Arctic climate change.

Acknowledgments. This publication is the result in part of research sponsored by the Cooperative Institute for Alaska Research with funds from the National Oceanic and Atmospheric Administration under Cooperative Agreement NA13OAR4320056 with the University of Alaska.

REFERENCES

Alexeev, V. A., E. S. Euskirchen, J. E. Cherry, and R. C. Busey, 2015: Tundra burning in 2007—Did sea ice retreat matter? *Polar Sci.*, **9**, 185–195, https://doi.org/10.1016/j.polar.2015.02.002.

Balzter, H., and Coauthors, 2005: Impact of the Arctic Oscillation pattern on interannual forest fire variability in central Siberia. *Geophys. Res. Lett.*, **32**, L14709, https://doi.org/10.1029/2005GL022526.

Cai, L., V. A. Alexeev, C. D. Arp, B. M. Jones, and V. E. Romanovsky, 2018: Modelling the impacts of projected sea ice decline on the low atmosphere and near-surface permafrost on the North Slope of Alaska. *Int. J. Climatol.*, https://doi.org/10.1002/joc.5741, in press.

Choi, D.-H., J.-S. Kug, W.-T. Kwon, F.-F. Jin, H.-J. Baek, and S.-K. Min, 2010: Arctic Oscillation responses to greenhouse warming and role of synoptic eddy feedback. *J. Geophys. Res.*, **115**, D17103, https://doi.org/10.1029/2010JD014160.

Collins, M., and Coauthors, 2013: Long-term climate change: Projections, commitments and irreversibility. *Climate Change 2013: The Physical Science Basis*, T. F. Stocker et al., Eds., Cambridge University Press, 1029–1136, http://www.ipcc.ch/pdf/assessment-report/ar5/wg1/WG1AR5_Chapter12_FINAL.pdf.

Compo, G. P., and Coauthors, 2011: The Twentieth Century Reanalysis Project. *Quart. J. Roy. Meteor. Soc.*, **137**, 1–28, https://doi.org/10.1002/qj.776.

Dee, D. P., and Coauthors, 2011: The ERA-Interim reanalysis: Configuration and performance of the data assimilation system. *Quart. J. Roy. Meteor. Soc.*, **137**, 553–597, https://doi.org/10.1002/qj.828.

Deser, C., 2000: On the teleconnectivity of ''Arctic Oscillation.'' *Geophys. Res. Lett.*, **27**, 779–782, https://doi.org/10.1029/1999GL010945.

Ebert, E. E., and J. L. McBride, 2000: Verification of precipitation in weather systems: Determination of systematic errors. *J. Hydrol.*, **239**, 179–202, https://doi.org/10.1016/S0022-1694(00)00343-7.

Gudkovich, Z., 1961: Relation of the ice drift in the Arctic Basin to ice conditions in the Soviet Arctic seas. *Tr. Okeanogr. Kom. Akad. Nauk SSSR*, **11**, 14–21.

Hollingsworth, A., K. Arpe, M. Tiedtke, M. Capaldo, and H. Savijärvi, 1980: The performance of a medium-range forecast model in winter–Impact of physical parameterizations. *Mon. Wea. Rev.*, **108**, 1736–1773, https://doi.org/10.1175/1520-0493(1980)108<1736:TPOAMR>2.0.CO;2.

Hu, Q., and S. Feng, 2010: Influence of the Arctic Oscillation on central United States summer rainfall. *J. Geophys. Res.*, **115**, D01102, https://doi.org/10.1029/2009JD011805.

Kay, J. E., and A. Gettelman, 2009: Cloud influence on and response to seasonal Arctic sea ice loss. *J. Geophys. Res.*, **114**, D18204, https://doi.org/10.1029/2009JD011773.

——, T. L'Ecuyer, A. Gettelman, G. Stephens, and C. O'Dell, 2008: The contribution of cloud and radiation anomalies to the 2007 Arctic sea ice extent minimum. *Geophys. Res. Lett.*, **35**, L08503, https://doi.org/10.1029/2008GL033451.

——, and Coauthors, 2015: The Community Earth System Model (CESM) Large Ensemble project: A community resource for studying climate change in the presence of internal climate variability. *Bull. Amer. Meteor. Soc.*, **96**, 1333–1349, https://doi.org/10.1175/BAMS-D-13-00255.1.

Kistler, R., and Coauthors, 2001: The NCEP–NCAR 50-Year Reanalysis: Monthly means CD-ROM and documentation. *Bull. Amer. Meteor. Soc.*, **82**, 247–267, https://doi.org/10.1175/1520-0477(2001)082<0247:TNNYRM>2.3.CO;2.

Krishnamurti, T. N., and Coauthors, 2003: Improved skill for the anomaly correlation of geopotential heights at 500 hPa. *Mon. Wea. Rev.*, **131**, 1082–1102, https://doi.org/10.1175/1520-0493(2003)131<1082:ISFTAC>2.0.CO;2.

Langland, R. H., and R. N. Maue, 2012: Recent Northern Hemisphere mid-latitude medium-range deterministic forecast skill. *Tellus*, **64A**, 17531, https://doi.org/10.3402/tellusa.v64i0.17531.

L'Heureux, M., A. Butler, B. Jha, A. Kumar, and W. Wang, 2010: Unusual extremes in the negative phase of the Arctic Oscillation during 2009. *Geophys. Res. Lett.*, **37**, L10704, https://doi.org/10.1029/2010GL043338.

Lindsay, R., M. Wensnahan, A. Schweiger, and J. Zhang, 2014: Evaluation of seven different atmospheric reanalysis products in the Arctic. *J. Climate*, **27**, 2588–2606, https://doi.org/10.1175/JCLI-D-13-00014.1.

Miller, R. L., G. A. Schmidt, and D. T. Shindell, 2006: Forced annular variations in the 20th century Intergovernmental Panel on Climate Change Fourth Assessment Report models. *J. Geophys. Res.*, **111**, D18101, https://doi.org/10.1029/2005JD006323.

Murphy, A. H., and E. S. Epstein, 1989: Skill scores and correlation coefficients in model verification. *Mon. Wea. Rev.*, **117**, 572–582, https://doi.org/10.1175/1520-0493(1989)117<0572:SSACCI>2.0.CO;2.

Ogi, M., S. Rysgaard, and D. G. Barber, 2016: Importance of combined winter and summer Arctic Oscillation (AO) on September sea ice extent. *Environ. Res. Lett.*, **11**, 034019, https://doi.org/10.1088/1748-9326/11/3/034019.

Overland, J. E., and M. Wang, 2010: Large-scale atmospheric circulation changes are associated with the recent loss of Arctic sea ice. *Tellus*, **62A**, 1–9, https://doi.org/10.1111/j.1600-0870.2009.00421.x.

——, J. A. Francis, E. Hanna, and M. Wang, 2012: The recent shift in early summer Arctic atmospheric circulation. *Geophys. Res. Lett.*, **39**, L19804, https://doi.org/10.1029/2012GL053268.

Phillips, A. S., C. Deser, and J. Fasullo, 2014: A new tool for evaluating modes of variability in climate models. *Eos, Trans. Amer. Geophys. Union*, **95**, 453–455, https://doi.org/10.1002/2014EO490002.

Poli, P., and Coauthors, 2016: ERA-20C: An atmospheric reanalysis of the twentieth century. *J. Climate*, **29**, 4083–4097, https://doi.org/10.1175/JCLI-D-15-0556.1.

Porter, D. F., J. J. Cassano, and M. C. Serreze, 2012: Local and large-scale atmospheric responses to reduced Arctic sea ice and ocean warming in the WRF model. *J. Geophys. Res.*, **117**, D11115, https://doi.org/10.1029/2011JD016969.

Rigor, I. G., J. M. Wallace, and R. L. Colony, 2002: Response of sea ice to the Arctic Oscillation. *J. Climate*, **15**, 2648–2663, https://doi.org/10.1175/1520-0442(2002)015<2648:ROSITT>2.0.CO;2.

Skeie, P., 2000: Meridional flow variability over the Nordic seas in the Arctic Oscillation framework. *Geophys. Res. Lett.*, **27**, 2569–2572, https://doi.org/10.1029/2000GL011529.

Steele, M., W. Ermold, and J. Zhang, 2008: Arctic Ocean surface warming trends over the past 100 years. *Geophys. Res. Lett.*, **35**, L02614, https://doi.org/10.1029/2007GL031651.

——, J. Zhang, and W. Ermold, 2010: Mechanisms of summertime upper Arctic Ocean warming and the effect on sea ice melt. *J. Geophys. Res.*, **115**, C11004, https://doi.org/10.1029/2009JC005849.

Stoner, A. M. K., K. Hayhoe, and D. J. Wuebbles, 2009: Assessing general circulation model simulations of atmospheric teleconnection patterns. *J. Climate*, **22**, 4348–4372, https://doi.org/10.1175/2009JCLI2577.1.

Taylor, K. E., R. J. Stouffer, and G. A. Meehl, 2012: An overview of CMIP5 and the experiment design. *Bull. Amer. Meteor. Soc.*, **93**, 485–498, https://doi.org/10.1175/BAMS-D-11-00094.1.

Thompson, D. W. J., and J. M. Wallace, 1998: The Arctic Oscillation signature in the wintertime geopotential height and temperature fields. *Geophys. Res. Lett.*, **25**, 1297–1300, https://doi.org/10.1029/98GL00950.

Tremblay, L.-B., 2001: Can we consider the Arctic Oscillation independently from the Barents oscillation? *Geophys. Res. Lett.*, **28**, 4227–4230, https://doi.org/10.1029/2001GL013740.

van der Linden, E. C., R. Bintanja, and W. Hazeleger, 2017: Arctic decadal variability in a warming world. *J. Geophys. Res. Atmos.*, **122**, 5677–5696, https://doi.org/10.1002/2016JD026058.

Vihma, T., P. Tisler, and P. Uotila, 2012: Atmospheric forcing on the drift of Arctic sea ice in 1989–2009. *Geophys. Res. Lett.*, **39**, L02501, https://doi.org/10.1029/2011GL050118.

Wang, J., and M. Ikeda, 2000: Arctic oscillation and Arctic sea-ice oscillation. *Geophys. Res. Lett.*, **27**, 1287–1290, https://doi.org/10.1029/1999GL002389.

——, J. Zhang, E. Watanabe, M. Ikeda, K. Mizobata, J. E. Walsh, X. Bai, and B. Wu, 2009: Is the dipole anomaly a major driver to record lows in Arctic summer sea ice extent? *Geophys. Res. Lett.*, **36**, L05706, https://doi.org/10.1029/2008GL036706.

Watanabe, E., J. Wang, A. Sumi, and H. Hasumi, 2006: Arctic dipole anomaly and its contribution to sea ice export from the Arctic Ocean in the 20th century. *Geophys. Res. Lett.*, **33**, L23703, https://doi.org/10.1029/2006GL028112.

Wu, B., J. Wang, and J. E. Walsh, 2006: Dipole anomaly in the winter Arctic atmosphere and its association with sea ice motion. *J. Climate*, **19**, 210–225, https://doi.org/10.1175/JCLI3619.1.

——, R. Zhang, and D. Rosanne, 2008: Arctic dipole anomaly and summer rainfall in northeast China. *Chin. Sci. Bull.*, **53**, 2222, https://doi.org/10.1007/s11434-008-0229-1.

——, J. E. Overland, and R. D'Arrigo, 2012: Anomalous Arctic surface wind patterns and their impacts on September sea ice minima and trend. *Tellus*, **64A**, 18590, https://doi.org/10.3402/tellusa.v64i0.18590.

Xin, X.-G., T.-J. Zhou, and R.-C. Yu, 2008: The Arctic Oscillation in coupled climate models. *Chin. J. Geophys.*, **51**, 223–239, https://doi.org/10.1002/cjg2.1214.

Yukimoto, S., and K. Kodera, 2005: Interdecadal Arctic Oscillation in twentieth century climate simulations viewed as internal variability and response to external forcing. *Geophys. Res. Lett.*, **32**, L03707, https://doi.org/10.1029/2004GL021870.

Zhang, J., R. Lindsay, M. Steele, and A. Schweiger, 2008: What drove the dramatic retreat of Arctic sea ice during summer 2007? *Geophys. Res. Lett.*, **35**, L11505, https://doi.org/10.1029/2008GL034005.

Zhang, R., 2015: Mechanisms for low-frequency variability of summer Arctic sea ice extent. *Proc. Natl. Acad. Sci. USA*, **112**, 4570–4575, https://doi.org/10.1073/pnas.1422296112.

Zhang, X., A. Sorteberg, J. Zhang, R. Gerdes, and J. C. Comiso, 2008: Recent radical shifts of atmospheric circulations and rapid changes in Arctic climate system. *Geophys. Res. Lett.*, **35**, L22701, https://doi.org/10.1029/2008GL035607.